



Parametric Analysis of Axially Loaded Partially Concrete-Filled Cold-Formed Elliptical Columns Subjected to Lateral Impact Load

Ghandi, E.^{1*}, Mohammadi Rana, N.² and Esmaeili Niari, SH.¹

¹ Associate Professor, Faculty of Technical and Engineering, University of Mohaghegh Ardabili, Ardabil, Iran.

² M.Sc., Faculty of Technical and Engineering, University of Mohaghegh Ardabili, Ardabil, Iran.

© University of Tehran 2023

Received: 04 Sep. 2023;

Revised: 28 Nov. 2023;

Accepted: 11 Dec. 2023

ABSTRACT: This research investigates the dynamic behavior of hollow and Partially Concrete-Filled Cold-Formed Steel Tubular (PCFCFST) columns that have elliptical cross-sections under simultaneous loading of dynamic lateral impact load and static compressive axial load. Utilizing Finite Element Analysis (FEA) by the ABAQUS is studied. In order to confirm the numerical modeling's precision, the study outcomes are compared to the outcomes of former experimental and numerical investigations. The effect of various factors namely aspect ratio, axial load ratio, impact angle, steel tube wall thickness, and concrete filling ratio on the performance of PCFCFST columns has been examined. The numerical analysis results indicate that specimens with higher concrete filling ratios show greater performance than hollow specimens. The columns' failure modes are significantly influenced by the impact angle and axial load ratio, particularly when the column aspect ratio is low. Surging the steel tube wall thickness from 2.25 mm to 4 mm decreases the maximum displacement by approximately 70%.

Keywords: Elliptical Section, Cold-Formed Steel, Lateral Impact, Partially Concrete-Filled Column.

1. Introduction

Recently, Concrete-Filled Steel Tubular (CFST) columns have become broadly utilized because of their ability to reduce the structures' weight, especially in docks, bridge piers, subway stations, and high-rise buildings. Fire resistance is an additional benefit of concrete-filled steel sections.

Steel sections have low fire resistance due to their definite heat capacity and high conductivity. The infilled concrete is like a sink, preventing temperature surges, and also the concrete has poor conductivity that

makes a high fire resistance (Rahnavard et al., 2022a; Craveiro et al., 2022; Moradi et al., 2021). Furthermore, building cost-effective and economical structures is one of the aims of structural design, while completely filling the column with concrete is an inefficient activity. Accordingly, in certain structures, concrete fills just the portions that are to be expected to be hit by impact, unless additional strength and ductility, particularly concerning earthquakes, are taken into account (Rondal, 2000; Yu, 2000). Today, the use of Cold-Formed Steel (CFS) cross-sections

* Corresponding author E-mail: ghandi@uma.ac.ir

because of their exceptional benefits, namely their high strength to weight ratio, ductility, fast fabrication, and installation, have been more considered in CFST columns. When the steel component is utilized as a part of the composite column, it indicates more compression strength compared to when it is utilized alone. This enhancement is because of the protection provided by the concrete filling, which prevents the cold-formed steel component from experiencing buckling deformation (Rahnavard et al., 2022b; Rahnavard et al., 2023). By elliptical hollow sections as fairly novel sections, both structural engineers and architectural designers are given further selections for having improved structural and aesthetics of the structure, respectively.

The bending capacity in these sections is more than the Circular Hollow Section (CHS) with a similar weight and size. These types of sections are also considered economical (Yang et al., 2017). Some investigations have been accomplished on CFT columns against impact loads. Yousuf et al. (2014) carried out numerical and experimental research on stainless steel columns and concrete-filled steel mild exposed to impact loading and transverse static with a pre-compressive axial load. The results indicated that the stainless steel specimens illustrate enhanced energy-dissipating features and higher strength in comparison with the mild steel columns.

Wang et al. (2015) presented a collective experimental, theoretical, and numerical research on the transverse for impact performance steel pipes filled with ultra-lightweight cement composite. Aghdamy et al. (2015) presented an investigation of the outcome of axially loaded concrete-filled cold-formed steel tube columns under lateral impact load with explicit nonlinear Finite Element (FE) methods. In general, they concluded that the CFST columns impact response is a significant factor that is heavily influenced by the slenderness ratio and tube thickness to diameter ratio (t/D).

Yang et al. (2015) studied a numerical

and experimental investigation of steel structures filled with Recycled Aggregate Concrete (RAC) under lateral impact loading behavior. The findings indicated that square RAC-filled steel tubular specimens have nearly equivalent lateral impact resistance as normal CFST counterparts. Shakir et al. (2015) investigated recycled and normal aggregate concrete-filled steel tube columns dynamic behavior exposed to lateral projectile impact and the influence of the Carbon Fiber-Reinforced Polymer (CFRP) jacketing on the structural performance of those columns.

Alam et al. (2016) performed numerical simulations to assess the influence of CFRP on concrete-filled steel tubular columns under vehicle impact loading. The dynamic impact analysis outcomes showed that adhesively attached CFRP sheets offer strengthened columns' enhanced impact resistance capacity by lessening lateral displacement by approximately 40% compared to normal CFST columns. Also, Han et al. (2019) examined the performance of stainless steel tubular columns and joints filled with concrete. They specifically focused on how these structures behaved when subjected to lateral and axial impact loads at both normal and elevated temperatures.

Zhu et al. (2018) examined the effect of lateral impact loads on cold-formed rectangular hollow steel columns filled with self-compacting concrete under lateral impact loads in both the front and corner directions. The results presented that the partially concrete-filled steel tubular specimens had much-improved behavior than the rectangular hollow steel tubular specimens. The concrete filling height influenced the failure mode remarkably, particularly when the specimens were verified under high-impact energy.

The impact direction and energy remarkably influenced the specimen's impact resistance. Xu et al. (2018) numerically investigated the anti-impact behavior of partially concrete-filled steel

tubular columns under lateral impact loading. The outcomes of parameter analysis indicated that the PCFST columns anti-impact performances remarkably surged when either the yield strength of steel or the concrete filling height rose significantly.

Zhang et al. (2019) examined the circular CFT columns' performance under compressive axial load and lateral impact loading. They concluded that lateral impact has adverse influences on the circular CFST columns' residual ultimate axial capacity. Residual ultimate axial capacity declines as impact energy surges and impact location approaches the end of the specimen. Furthermore, research has shown that the compressive strength of concrete might mitigate the negative effects of the impact site on the remaining maximum axial capacity. Wan et al. (2017) examined the lateral impact loading's effect on the residual axial strength of CHS columns. The outcomes designated that lateral impact significantly influences the axial compression behavior of CHS columns. When the impact energy increases, the residual axial strength is reduced, and the lateral plastic deformation increases. Additionally, the outcomes indicate that CHS columns axial bearing capacity is significantly influenced by the impact location.

Du et al. (2018) investigated the remaining axial bearing capacity of Concrete-Filled Circular Steel Tubular Columns (CFCSTCs) following transverse impact stress. In some studies, CFT columns with elliptical cross-sections have been studied. The outcomes indicated that the impact height and the outer diameter to thickness of the outer steel tube ratio have obvious impacts on the CFCSTCs axial compression behavior. The samples failure mode is usually local buckling. Furthermore, the maximum lessening of the columns axial bearing capacity attains approximately 35% in comparison with that of untreated columns.

The numerical and experimental

investigations carried out by Liu et al. (2017) refer to the investigation of the behavior of concrete-filled cold-formed elliptical sections with different aspect ratios under axial compression load. The findings demonstrated that the design approach advocated in the Chinese Standard (GB50936-2014), as well as the design strategy for circular CFST columns in EC4, yielded precise forecasts. Wang et al. (2018) considered the behavior of elliptical concrete-filled thin-walled steel tube columns (ECFT) under compressive axial load by FE modeling with ABAQUS software. The analysis outcomes indicated that the confinement factor influences the axial force-axial displacement curves of the elliptical concrete-filled thin-walled steel tube stub columns. Finally, two simplified design approaches were proposed to predict the axial compressive capacities of elliptical concrete-filled thin-walled steel tube columns, on the basis of the unified theory approach and simple superposition approach.

Numerous numerical and experimental researches have been executed on CFT columns regarding different sections and loads. Nevertheless, as can be perceived from the above-mentioned investigations, the performance of elliptical hollow and PCFCFST columns under simultaneous loading of lateral impact load and axial static compressive load is not studied. Consequently, the lateral impact response of elliptical hollow and PCFCFST axially loaded columns by considering the effect of different factors, namely impact shape, impact velocity, impact block mass, impact block size, impact angle, and height were investigated by Mohammadi Rana et al. (2021).

In this paper, the previous work of Mohammadi Rana et al. (2021) is extended by studying the effect of aspect ratio, axial load ratio, concrete filling ratio, and steel tube wall thickness on the response of elliptical PCFCFST columns under simultaneous loading of lateral impact load and axial static compressive load.

ABAQUS, as the FE software (ABAQUS/CAE 6.13) is used for numerical modeling and investigating the effect of various parameters.

2. Numerical Modeling

Figure 1 depicts the characteristics of the studied PCFCFST columns with elliptical cross-sections under simultaneous loading of lateral impact load and axial static compressive load. The column consists of a steel tube with an elliptical cross-section and a concrete core with height h_c . The column is first subjected to a compressive axial load N , and then a lateral impact load is employed at the height of h_0 from the lower support of the column. The lateral impact is applied by an impact block. The performance of the columns is investigated by two types of analysis (Static/General and Dynamic/Explicit).

Static/General analysis is utilized to specify the columns under axial compressive loading's ultimate axial load capacity. The lateral impact loading is

determined by Dynamic /Explicit analysis. Both types of analysis are performed by considering geometric and material nonlinearities. The features of concrete material in ABAQUS software are defined by 2 types of behavior: plastic and elastic.

The elastic properties of concrete were characterized using Young's modulus and Poisson's ratio. The present investigation employed self-compacting concrete, as described by Liu et al. (2017, for the purpose of filling cold-formed steel tubes. For replicating the nonlinear performance of concrete in ABAQUS, the Concrete Damage Plasticity (CDP) model was also assumed. Specifications of concrete and cold-formed steel materials and details of their modeling has been given in Mohammadi Rana et al. (2021). The eight-node hexagonal solid element (C3D8R) is utilized to model core concrete, stiffeners, and end plates involved in columns. In order to model the steel tube, the 4-node shell element (S4R) with 6 degrees of translational and rotational freedom in every node and reduced integration has been used.

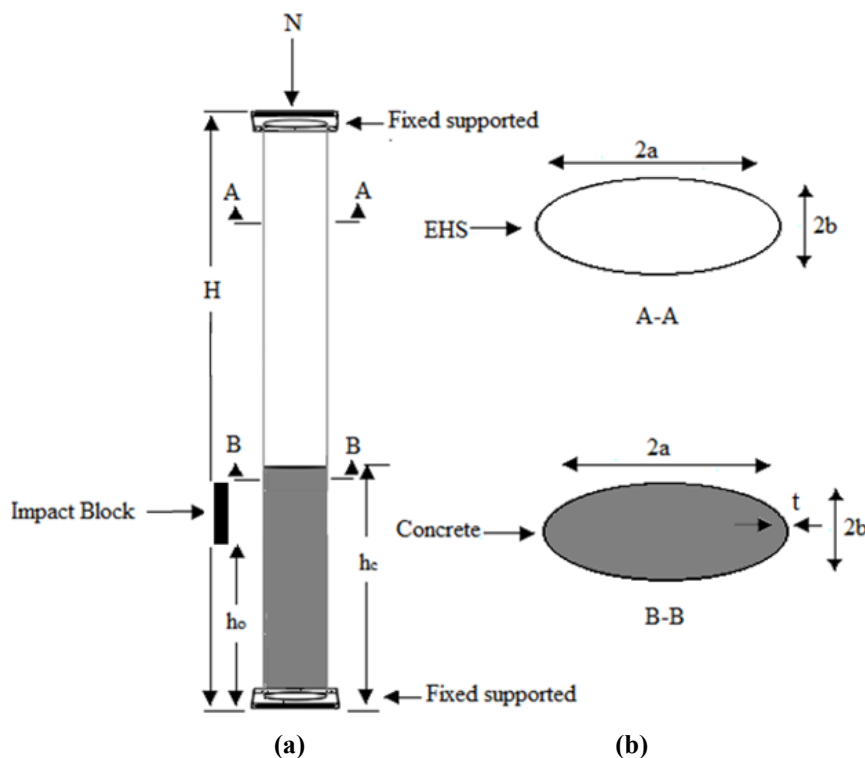


Fig. 1. Characteristics of the studied columns: a) The general view of the column at height (H : is the total length of the steel tube, h_c : is the concrete filling height, and h_0 : location of lateral impact load); and b) Cross-section of the studied columns

The R3D4 solid stiff element is utilized to simulate the impact block. In a FEA, the contact conditions allow the force to be transferred from one part of the model to another. In composite columns, the force is transmitted between concrete and steel through contact between these two materials. The surface-to-surface contact element is used to model the contact between the concrete part and the steel tube and between the column and the impact block. This element defines the contact between a deformable surface and a rigid surface or between 2 deformable surfaces.

The parameters utilized to apply the contact features between steel and concrete are as follows:

(Normal behavior): Considering the hard contact between the concrete and the steel surface, the penetration of the concrete surface into the steel surface is allowed to a minimum and does not allow the transfer of tensile stress during the interaction, and only the pressure on the two surfaces transfer by contact, and when it separates, there is no pressure between the two surfaces.

(Tangential Behavior): The Columbus friction model was utilized to model the tangential and sliding behavior of the two surfaces. The penalty option is defined to determine the friction factor between steel surfaces and concrete. The friction factor between steel surfaces and concrete is considered as 0.47 (Baltay and Gjelvik, 1990). The initial geometrical imperfection was considered for steel hollow sections as the lowest buckling mode shape with an amplitude of $t_s/100$, in which t_s : is defined as the tube wall thickness. In the FE model, residual stresses were not calculated and were not regarded.

The effect of local imperfections and residual stress for CFST stub columns are insignificant because of the inner concrete, and consequently, these factors were not considered in the Finite Element (FE) model (Liu et al., 2017). In order to simulate boundary conditions, total degrees of freedom at the lower end plate were limited,

and the load transfer in the axial direction was carried out by rigid plates. Rectangular end plates with a uniform thickness of 20 mm have been utilized in entire specimens.

In this paper, the columns are exposed to axial loading without eccentricity. The compressive axial load is applied as a displacement control method in Static/General analysis. A rectangular stiff body with dimensions of 150 mm × 400 mm and 3750 J impact energy, which is located at a lateral distance of 300 mm from the columns, was used for impact block modeling. The position of lateral impact is $\frac{1}{3}$ of column height. For applying the impact load on the column, the impact block is modeled with an initial mass and velocity.

The velocity option in the Predefined field is used to define the initial velocity of the impact. For this purpose, a constant mass impact block weighing 300 kg is utilized to apply a consistent impact load at a velocity of 5 m/s.

3. Validation of the FE model

To ensure the precision of numerical modeling, first, a PCFCFST column with a rectangular cross-section under lateral impact loading (first model: Zhu et al. (2018)) and then a PCFCFST column with elliptical cross-section under axial compression loading (second model: Liu et al. (2017)) are modeled in ABAQUS, and the results of numerical modeling are compared with the outcomes of the former studies in mentioned references. The first model has a rectangular cross-section with rounded corners, which has been impacted once by a lateral impact load from the front and again from the corner. The total height of the column is 1500. The impact block has an average velocity of 6.5 m/s, which hits the column at a height of 320 mm.

Details of the verification of the first model are given in the authors' former work (Mohammadi Rana et al., 2021). As an example of the verification results of this model, displacement - time curves of PCFCFST specimen with the concrete

filling height of 400 mm under front impact load and PCFCFST specimen with the concrete filling height of 700 mm under corner impact load in numerical modeling and experimental tests are compared in Figure 2 and Table 1. Figure 2 and Table 1 indicate a strong concurrence between the numerical results of the present study and the experimental and numerical findings of Zhu et al. (2018), affirming the precision of the numerical modeling employed in this study.

The observed difference between the experimental and numerical findings can be related to the friction between the devices and the interference of environmental factors in the laboratory conditions, which are not considered in the numerical

modeling. The second model is a concrete-filled cold-formed steel elliptical column under a compressive axial load. The aspect ratios (a/b) of cold-formed elliptical steel sections vary from 1 to 2.5. The ratio between the cross-sectional area of the steel tube and the cross-sectional area of the concrete core ($\alpha_s = A_s/A_c$) is defined between 5 and 12%. Cold-formed steel sheets with a thickness of 2.75 mm have been used for the column tubes. Figure 3 depicts the geometric model of the column that is created in ABAQUS. In this model, the axial load is applied as a displacement control at the center of the upper rigid plate, in the direction of the column axis.

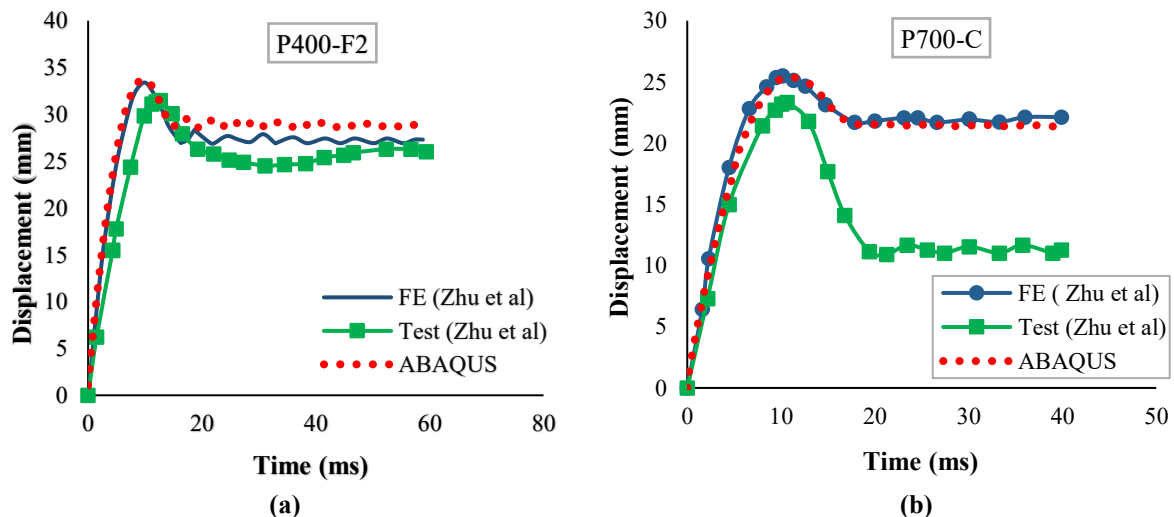


Fig. 2. Displacement - time curves of PCFCFST specimens: a) Concrete filling height of 400 mm under front impact load; and b) Concrete filling height of 700 mm under corner impact load

Table 1. Quantitative comparison between Zhu et al. (2018) results and ABAQUS results of this research

Specimen	Test ^a Zhu et al. (2018)	Peak displacement (mm)			t_d (ms) (duration from initial impact to the Δ_{max})		FE ^c Zhu et al. (2018)	ABAQUS ^f	Error (%)	
		FE ^b Zhu et al. (2018)	ABAQUS ^e	Error (%)	Test ^d Zhu et al. (2018)	FE ^c Zhu et al. (2018)			(c-a)/a	(c-b)/b
P400-F2	31.49	33.59	33.75	7.20	-0.48	12.68	10.89	11.00	-13.9	1.07
P700-C	32.60	33.40	31.28	-3.41	-5.73	10.62	10.17	11.00	3.49	8.14

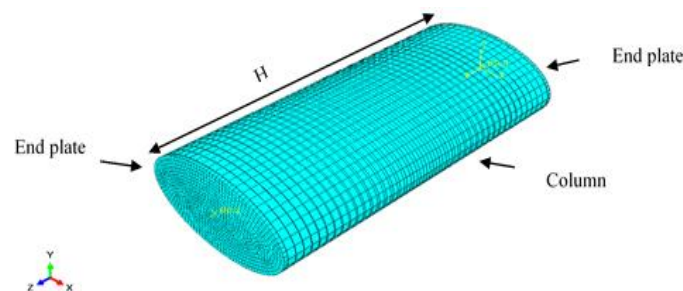


Fig. 3. CFT column meshes modeled in ABAQUS

The dimensions of every mesh size in the model range from 5 to 10 mm. The steel tube and concrete were modeled, in turn, with four-nodded shell element S4R and eight-nodded solid element C3D8R. The dimensions of the cold-formed hollow steel column are $2a = 203.3$ mm, $2b = 101.6$ mm (CH20-a) and $H = 407$ mm. Also, the concrete-filled column with the same dimensions as the hollow column (C20-8-a) and with α_s ratio equal to 8% is considered. The distinction between the experimental and numerical outcomes of Liu et al. (2017) with the numerical results of this paper in the form of axial displacement - load curves in Figure 4 and the difference ratio in Table 2 shows a qualified agreement between the outcomes.

4. Parametric Studies

The behavior of PCFCFST columns under simultaneous compressive lateral impact and axial load depends on many parameters.

In this paper, the influence of aspect

ratio ($R = a/b$), compressive axial load ratio ($N = n/N_{u,F}$) (n : is the compressive axial load on the column, $N_{u,F}$: is the ultimate axial compressive capacity of the partially concrete-filled steel column), the impact angle (A), the concrete filling ratio (P) and steel tube thickness (T) are investigated on the behavior of the mentioned columns.

In this study, the columns will first be exposed to compressive axial load to obtain the ultimate axial bearing capacity of the columns with diverse filling ratios. The columns will then be exposed to lateral impact loads simultaneously with the axial compressive load.

Figure 5 depicts the impact angles. For investigating the effect of different factors on the behavior of PCFCFST columns, an entire 51 specimens have been investigated, the naming pattern of which is given in Figure 6. The general features of the specimens are illustrated in Table 3. In the current paper, the column has an entire height of 3600 mm.

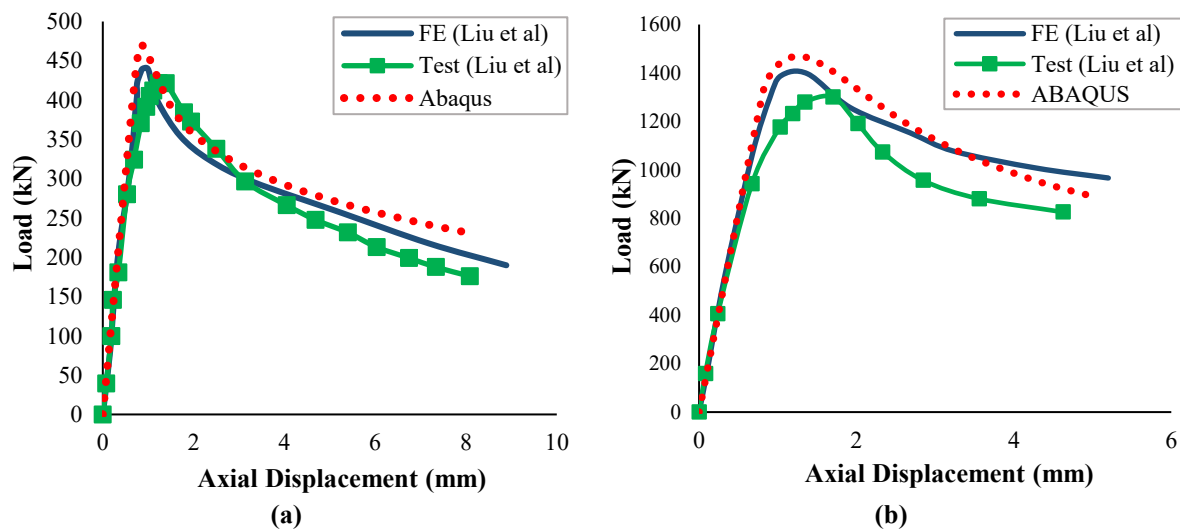


Fig. 4. Axial displacement - load curves of elliptical hollow column: a) (CH20-a); and b) (C20-8-a)

Table 2. Quantitative comparison between Liu et al. (2017) results and ABAQUS results of this paper

Specimen	Test ^a Liu et al. (2017)	Peak load (kN)			Error (%) (c-a)/ a	Δu (mm) (displacement at peak load)			Error (%) (f-d)/d	Error (%) (f-e)/e
		FE ^b Liu et al. (2017)	ABAQUS ^c	Error (%) (c-b)/b		Test ^d Liu et al. (2017)	FE ^e Liu et al. (2017)	ABAQUS ^f		
CH20-a	439.81	421.29	470.48	11.58%	6.89%	1.23	0.87	0.83	32.50	4.78
C20-8-a	1300.46	1396.4	1466.52	12.76%	5.01%	1.78	1.38	1.34	24.71	3.33

4.1. Static Analysis of the Columns to Specify the Ultimate Bearing Capacity

This section's goal is to specify the PCFCFST columns' ultimate compressive bearing capacity. First, the analysis of entirely concrete-filled elliptical steel columns under compressive axial load is performed, and the columns axial bearing capacity has been obtained. Then, to ensure the precision of the analysis, the calculated axial bearing capacity is compared with Eq. (1) result that computes the columns' axial bearing capacity based on the EC4 (Zhang et al., 2019):

$$N_{u,EC4} = f_y A_s + \hat{f}_c A_c \quad (1)$$

where f_y and \hat{f}_c : are the yield strength of steel and the compressive strength of concrete, respectively. Also, A_s and A_c : are the steel and concrete's cross-sectional area, respectively.

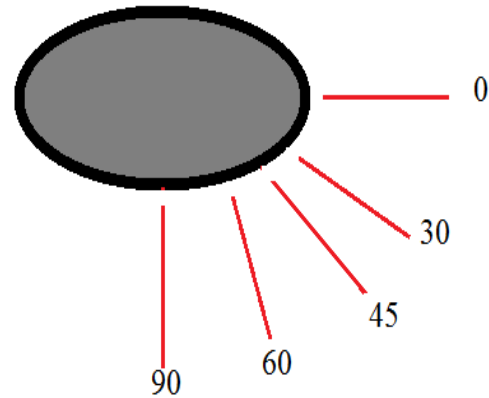


Fig. 5. Impact angles (degree)

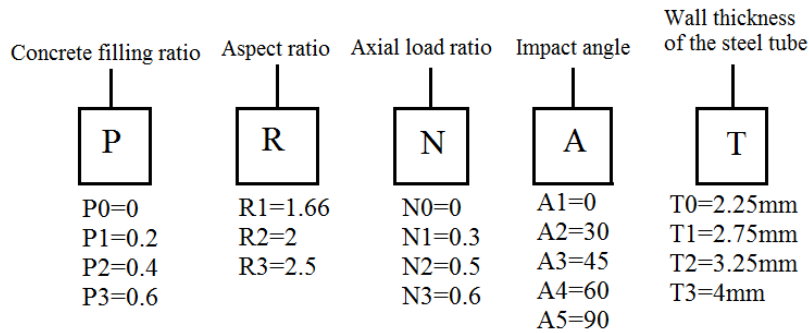


Fig. 6. The naming pattern of the studied specimens

Table 3. Detailed information on each specimen

Specimen Name	P	R	N	A(Degree)	T(mm)	Specimen Name	P	R	N	A(Degree)	T(mm)
P0R1N2A2T1	0	1.66	0.5	0	2.75	P2R3N2A5T1	0.4	2.5	0.5	90	2.75
P1R1N2A2T1	0.2	1.66	0.5	0	2.75	P2R1N0A2T1	0.4	1.66	0	30	2.75
P2R1N2A2T1	0.4	1.66	0.5	0	2.75	P2R1N1A2T1	0.4	1.66	0.3	30	2.75
P3R1N2A2T1	0.6	1.66	0.5	45	2.75	P2R1N2A2T1	0.4	1.66	0.5	30	2.75
P0R2N2A2T1	0	2	0.5	45	2.75	P2R1N3A2T1	0.4	1.66	0.6	30	2.75
P1R2N2A2T1	0.2	2	0.5	45	2.75	P2R2N0A2T1	0.4	2	0	30	2.75
P2R2N2A2T1	0.4	2	0.5	0	2.75	P2R2N1A2T1	0.4	2	0.3	30	2.75
P3R2N2A2T1	0.6	2	0.5	0	2.75	P2R2N2A2T1	0.4	2	0.5	30	2.75
P0R3N2A2T1	0	2.5	0.5	0	2.75	P2R2N3A2T1	0.4	2	0.6	30	2.75
P1R3N2A2T1	0.2	2.5	0.5	45	2.75	P2R3N0A2T1	0.4	2.5	0	30	2.75
P2R3N2A2T1	0.4	2.5	0.5	45	2.75	P2R3N1A2T1	0.4	2.5	0.3	30	2.75
P3R3N2A2T1	0.6	2.5	0.5	45	2.75	P2R3N2A2T1	0.4	2.5	0.5	30	2.75
P2R1N2A1T1	0.4	1.66	0.5	0	2.75	P2R3N3A2T1	0.4	2.5	0.6	30	2.75
P2R1N2A2T1	0.4	1.66	0.5	30	2.75	P2R1N2A2T0	0.4	1.66	0.5	30	2.25
P2R1N2A3T1	0.4	1.66	0.5	45	2.75	P2R1N2A2T1	0.4	1.66	0.5	30	2.75
P2R1N2A4T1	0.4	1.66	0.5	60	2.75	P2R1N2A2T2	0.4	1.66	0.5	30	3.25
P2R1N2A5T1	0.4	1.66	0.5	90	2.75	P2R1N2A2T3	0.4	1.66	0.5	30	4
P2R2N2A1T1	0.4	2	0.5	0	2.75	P2R2N2A2T0	0.4	2	0.5	30	2.25
P2R2N2A2T1	0.4	2	0.5	30	2.75	P2R2N2A2T1	0.4	2	0.5	30	2.75
P2R2N2A3T1	0.4	2	0.5	45	2.75	P2R2N2A2T2	0.4	2	0.5	30	3.25
P2R2N2A4T1	0.4	2	0.5	60	2.75	P2R2N2A2T3	0.4	2	0.5	30	4
P2R2N2A5T1	0.4	2	0.5	90	2.75	P2R3N2A2T0	0.4	2.5	0.5	30	2.25
P2R3N2A1T1	0.4	2.5	0.5	0	2.75	P2R3N2A2T1	0.4	2.5	0.5	30	2.75
P2R3N2A2T1	0.4	2.5	0.5	30	2.75	P2R3N2A2T2	0.4	2.5	0.5	30	3.25
P2R3N2A3T1	0.4	2.5	0.5	45	2.75	P2R3N2A2T3	0.4	2.5	0.5	30	4
P2R3N2A4T1	0.4	2.5	0.5	60	2.75						

Figure 7 depicts an overview of the investigated specimens created in ABAQUS software. In this section, for each aspect ratio (R), four filling heights have been considered, and in each case, a Static/General analysis has been performed. An initial geometric imperfection has been regarded in the static analysis, which is according to the columns first buckling mode under compressive axial load.

Table 4 indicates the columns axial compressive capacity (N_u) and is compared with the axial capacity calculated with Eq. (1) ($N_{u,EC4}$) for filling ratio $P=1$. As can be seen from this table, the consistency of the results is well. Also, partially concrete-filled columns have a lower capacity than completely concrete-filled columns. Figure 8 demonstrates the axial load-axial displacement curves of the columns with

different aspect ratios R and filling ratios P.

It can be seen that for each aspect ratio, the ultimate axial capacity of columns with different filling ratios are close to each other approximately and the rate of increase of the column stiffness with rising the column filling ratio is different in each case. It is also observed that for the same filling ratio, the columns ultimate axial capacity surges with a rising aspect ratio.

According to the performed studies (Mohammadi Rana et al., 2021) and observing the significant effect of compressive axial load on the lateral deflection of partially concrete-filled columns under lateral impact loading, in the present study, 50% of column's the ultimate axial capacity in Table 4 (N_u) is considered as the compressive axial load.

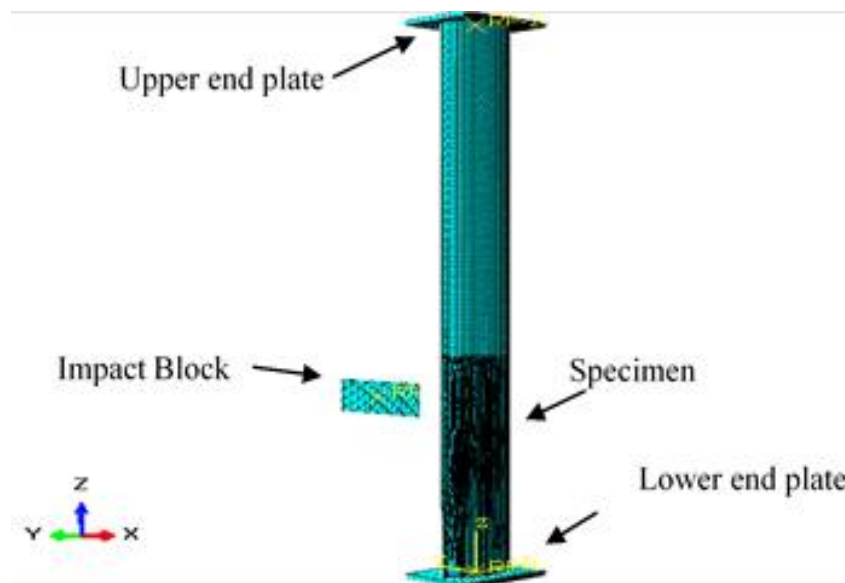


Fig. 7. An overview of the studied specimens created in ABAQUS

Table 4. The ultimate capacity of the columns with different aspect ratios and filling ratios

$a \times b$	A_s (mm^2)	A_c (mm^2)	R	P	$N_{u,EC4}$ (N) Eq.(1)	N_u (N) (ABAQUS)
100×60	1358.4	17491	1.66	0.2	-	383981
				0.4	-	389559
				0.6	-	397594
				1	1103781	1067300
				0.2	-	528847
150×75	1920.3	33423	2	0.4	-	536722
				0.6	-	539978
				1	1864845	1850830
				0.2	-	541631
				0.4	-	568498
250×100	3000.3	75539	2.5	0.6	-	587518
				1	3729865	3713870

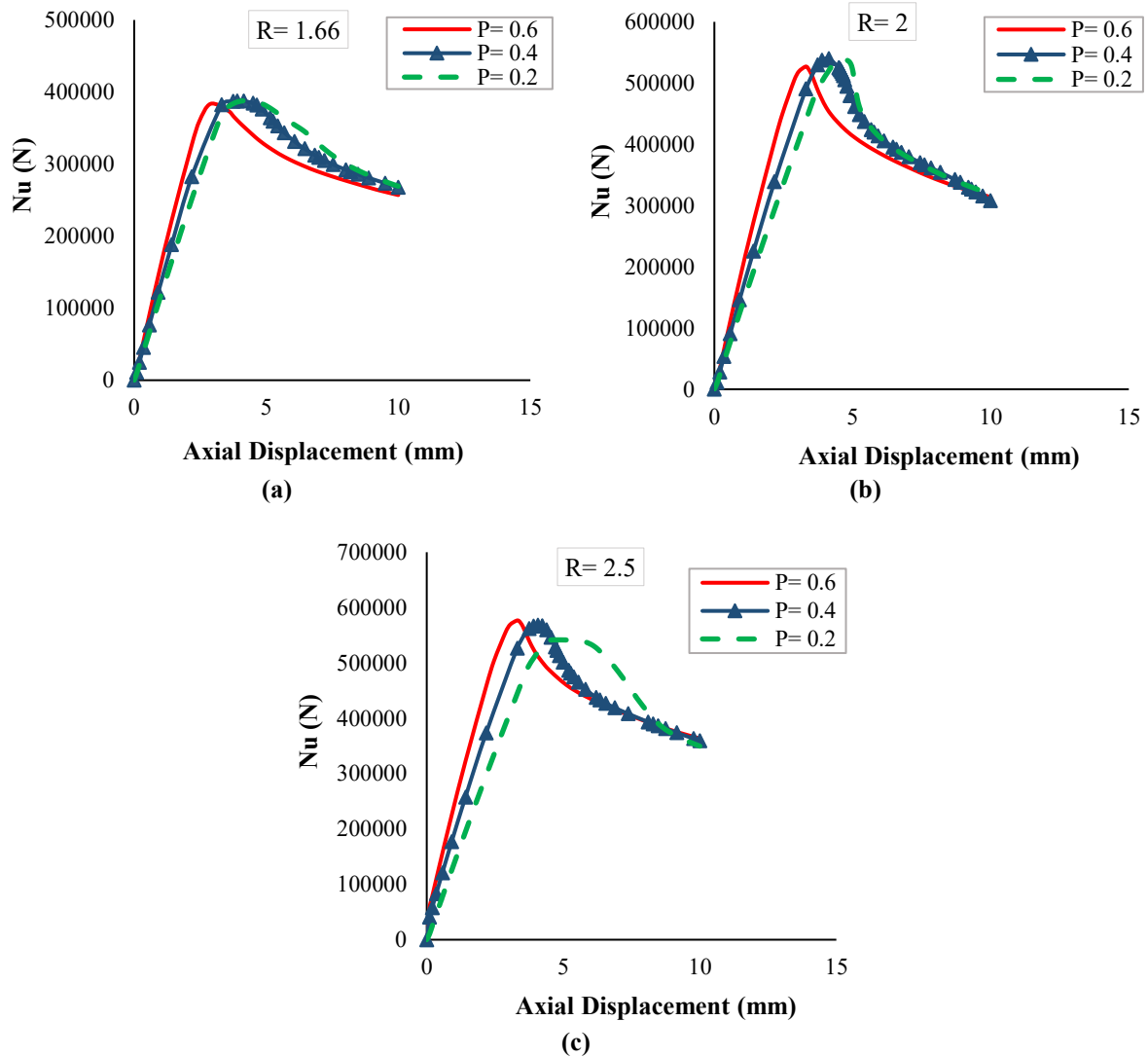


Fig. 8. Axial load - axial displacement curves of specimens with different aspect ratios R and different filling ratios P

4.2. Concrete Filling Ratio Effect

The aim of this section is to scrutinize the influence of the concrete filling ratio on the behavior of PCFCFST columns under lateral impact loading. In the present study, three ratios of filling 0.2, 0.4, and 0.6 have been selected to study the influence of filling ratio (P). Also, cold-formed steel hollow sections have been analyzed for comparison. In the analysis of this section, the impact angle has been considered A2 (30°). Considering the aspect ratios R1, R2, and R3, it can be said that for each aspect ratio, four specimens have been analyzed.

The specifications of the 12 specimens considered in this section are obtained from Table 3. The specimens were subjected to simultaneous loading of compressive axial

load and lateral impact load and were analyzed by dynamic/explicit analysis. Figures 9-11 display the analysis results in the form of displacement-time curves, impact force-time curves, and failure modes, respectively. The output of the analysis is extracted at the opposite point of the impacted region in the direction of the impact. Based on Figure 9, it is clear that with increasing filling ratio, the displacements decrease. It also reduces the time to reach the maximum displacement (Δ_{max}). The displacement increases linearly up to t_d (duration from initial impact to the Δ_{max}) and after the Δ_{max} point, vibrates a little, attaining a relatively stable amount.

Maximum values of t_d and Δ_{max} are 36.176 (MS) and 96.1686 mm, respectively.

Both of which are related to the P0R1N2A2T1 specimen. By Comparing the bar charts in Figure 9d, it is evident that hollow columns have the highest Δ_{max} for the different aspect ratios, and columns with the highest filling ratio (0.6) have the lowest Δ_{max} . Figure 10 demonstrates the increase in impact force with increasing filling ratio and aspect ratio.

The maximum impact force is 408.43 kN, connected to the P3R3N2A2T1 specimen. Based on the diagrams in Figure 10, it can be noticed that the force-time curves consist of three stages. First, the impact force at the moment of impact quickly reaches its maximum value, and this procedure is explained as the peak stage. After that, the impact force decreases to an oscillation level, and after fluctuations that occur after the peak, the amount of

force remains almost constant (especially in the filling ratios P0 and P1).

By the impact energy dissipation, the impact force slowly reaches 0, called the final stage. Furthermore, the results show that the lower the filling ratio, the duration of contact between the column and impact block is longer and the lower the impact load. Figure 10d indicates that with rising the filling ratio, the maximum impact force also increases, and at larger filling ratios, the effect of the aspect ratio on increasing the maximum impact force is more noticeable. Of all the specimens studied in this section, specimens with R1 aspect ratio have the highest deformation under impact load. Therefore, the failure modes of specimens with R1 impact ratio for different filling ratios are revealed in Figure 11.

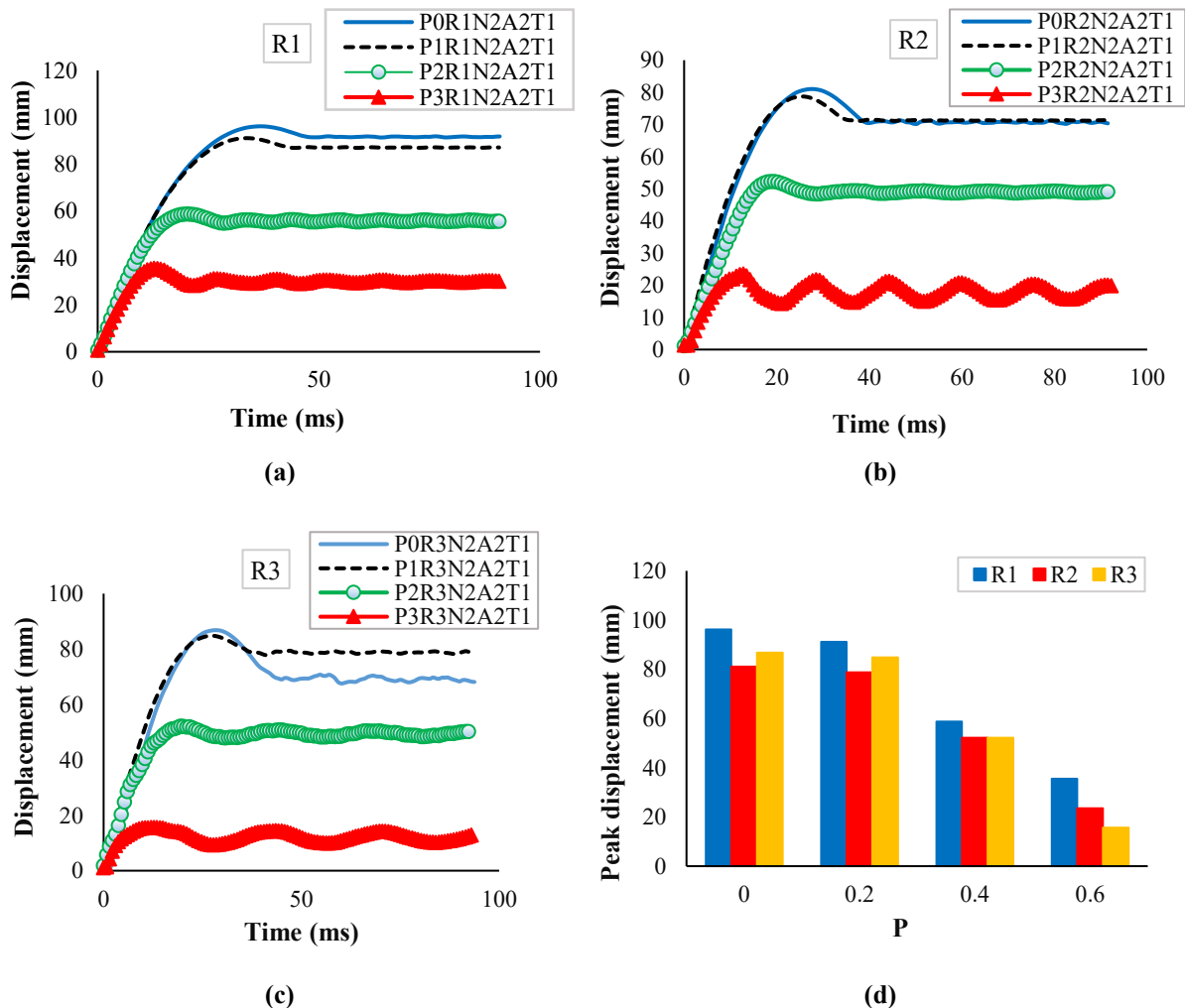


Fig. 9. The displacement - time curves of the columns with different filling ratios: a) Aspect ratio R1; b) Aspect ratio R2; c) Aspect ratio R3 ;and d) Comparison of peak displacements

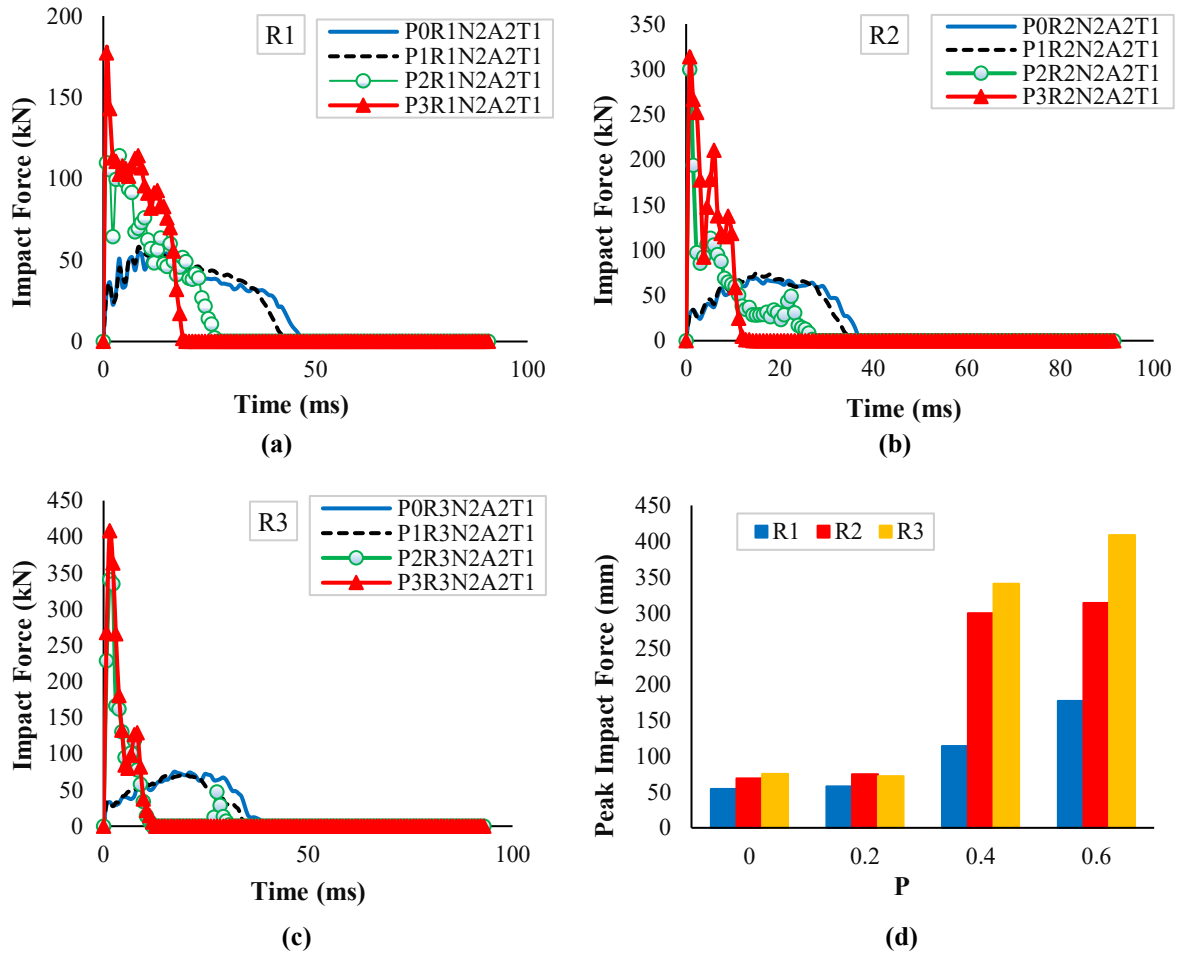


Fig. 10. The impact force-time curves of columns with different filling ratios: a) Aspect ratio R1; b) Aspect ratio R2; c) Aspect ratio R3; and d) Comparison of peak impact forces

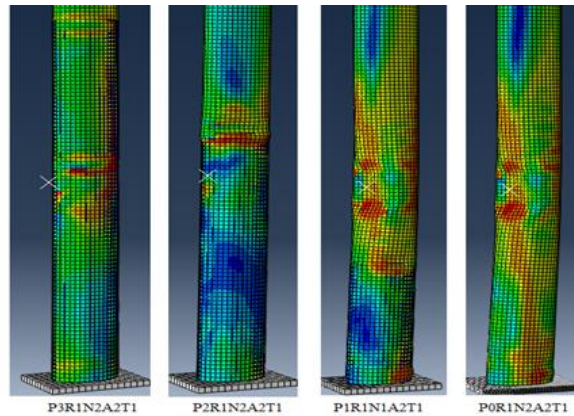


Fig. 11. The failure modes of the columns with the R1 aspect ratio with different filling ratios

It is clear that the specimen with a filling ratio of P0 has the maximum deformation, and the specimen with the highest filling ratio ($P3 = 0.6$) has the minimum deformation.

4.3. The Effect of Impact Angle

The primary aim of this section is to examine the effect of impact angle on the

performance of elliptical PCFCFST columns. In this research, the influence of impact angle (A) is investigated by considering five angles of 0, 30, 45, 60, and 90 degrees, as demonstrated in Figure 5. In the analysis of this part, the filling ratio is considered P2, and the aspect ratios are R1, R2 and R3. The specifications of the 15 specimens considered in this section are

gained from Table 3. Having applied the lateral impact load, the analyses' results which include displacement-time curves in Figure 12, impact force-time curves in Figure 13, and failure modes in Figure 14, are illustrated. Based on Figure 12, it is clear that at the impact angle of A1 (0°), where the impact is applied along the large diameter of the ellipse section, the displacements created at the impact block is opposite point are far less than the displacements at other impact angles, so that the maximum amount of displacements occurs at the impact angle A5 (90°) along the ellipse section's small diameter. The P2R1N2A5T1 type is associated with a maximum displacement of 89.85 mm. In the R1 and R2 aspect ratios for all impact angles, first, the displacements surge linearly up to the peak point, and after that, displacements become relatively stable.

However, in the R3 aspect ratio,

displacements increase linearly up to the peak point, but after that, it is accompanied by an oscillating state. The increasing trend of maximum displacement by increasing the impact angle can be seen in the bar chart of Figure 12d.

It is also observed that by altering the impact angle from A1 (0°) to A5 (90°), the increase in displacement in the R3 aspect ratio is much less than the R1 and R2 aspect ratios. According to Figure 13, it is clear that for all impact angles, the impact force increases with surging aspect ratio, and for a fixed aspect ratio, the impact force also rises with increasing impact angle from A1 (0°) to A5 (90°). The greatest impact force of 701.639 kN is associated with the P2R3N2A5T1 specimen. Also, as the impact angle increases, the duration of contact between the impact block and column is extended following the collision.

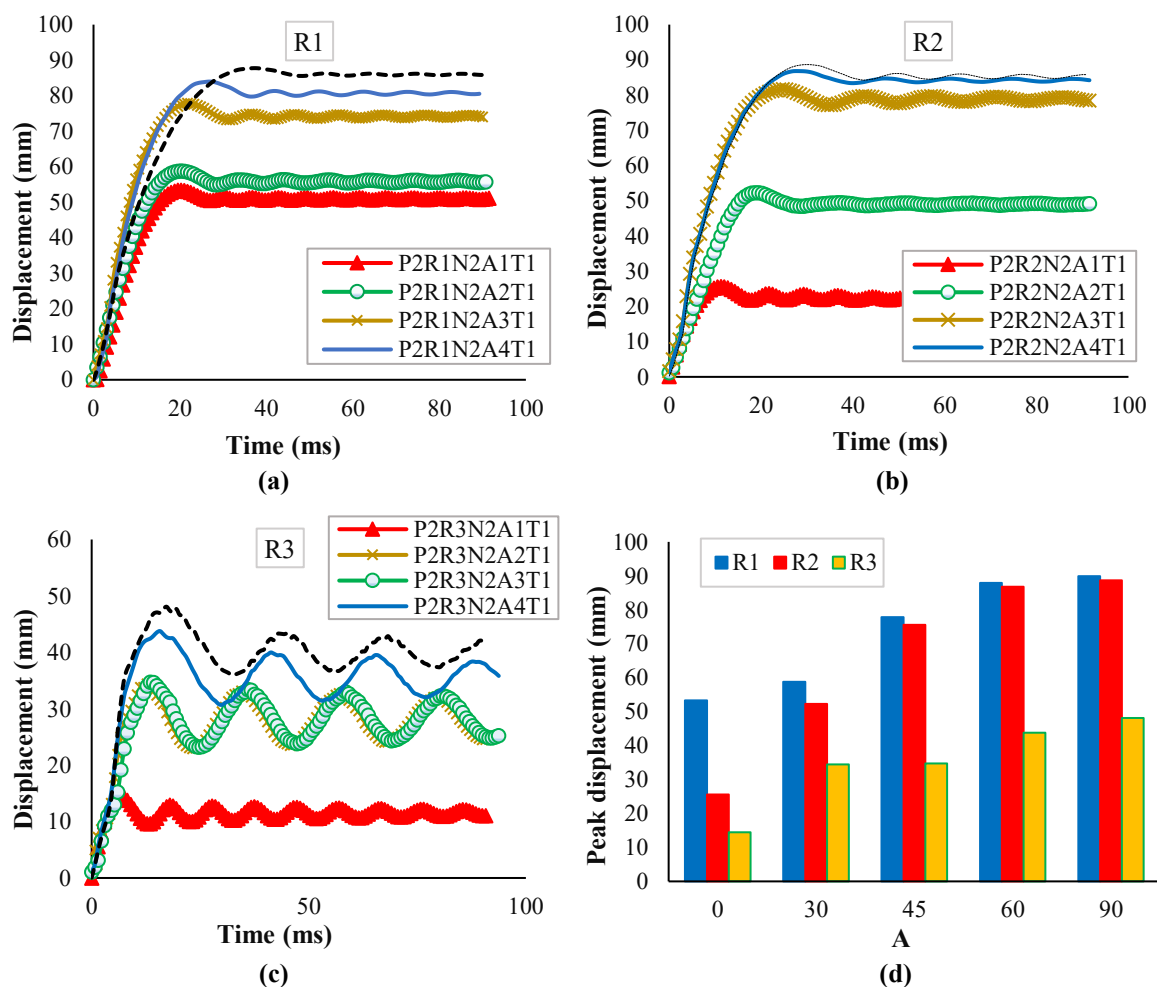


Fig. 12. The displacement - time curves of columns with different impact angles: a) Aspect ratio R1; b) Aspect ratio R2; c) Aspect ratio R3; and d) Comparison of peak displacements

From the bar chart of Figure 13d, the correlation between the maximal impact force and the impact angle and aspect ratio is apparent. The failure modes of specimens with an R1 aspect ratio for the five different impact angles are revealed in Figure 14. It is evident from Figure 14 that the maximum displacement is related to the impact angle of A5 (90°). The impact angle A2, the filling

ratio P2, and the aspect ratios R1, R2, and R3 are considered.

Therefore, it can be said that for each aspect ratio, four specimens have been analyzed. The findings from the analysis of displacement-time curves are presented in Figure 15, while the impact force-time curves are depicted in Figure 16.

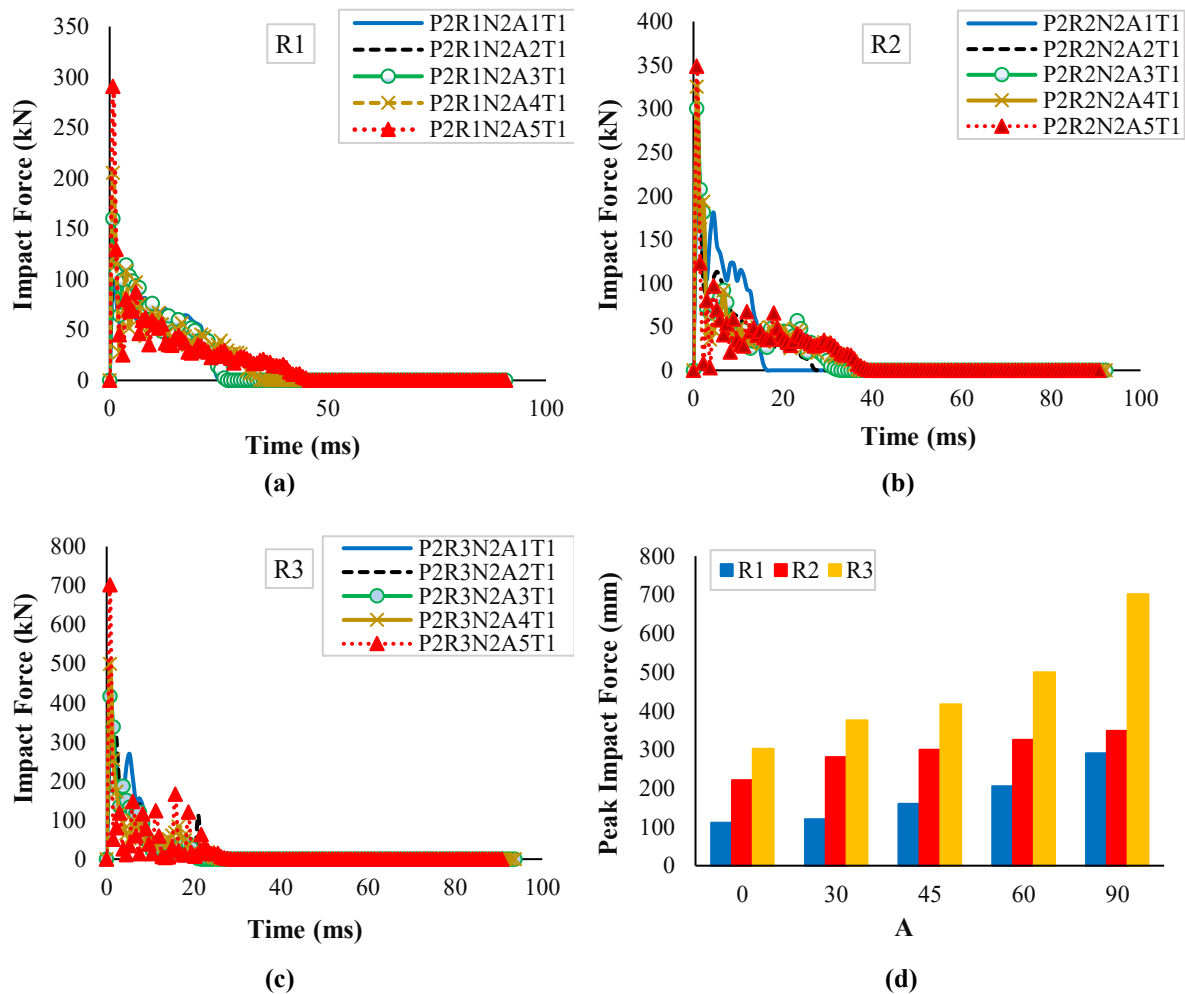


Fig. 13. The impact force-time curves of columns with different impact angles: a) Aspect ratio R1; b) Aspect ratio R2; c) Aspect ratio R3; and d) Comparison of peak impact forces

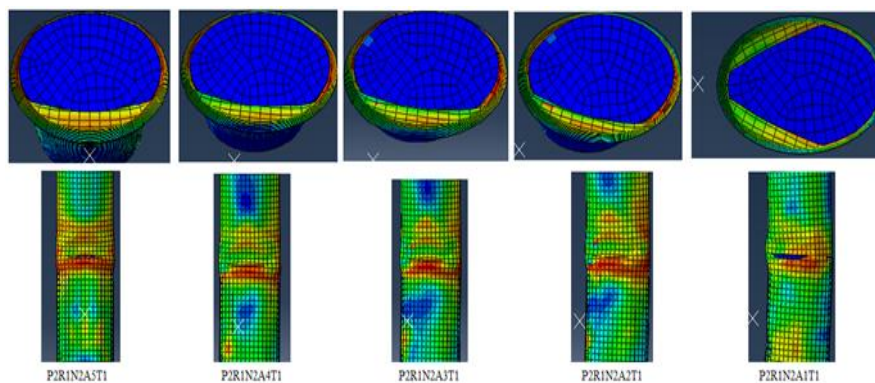


Fig. 14. The failure modes of the columns with the R1 aspect ratio with different impact angles

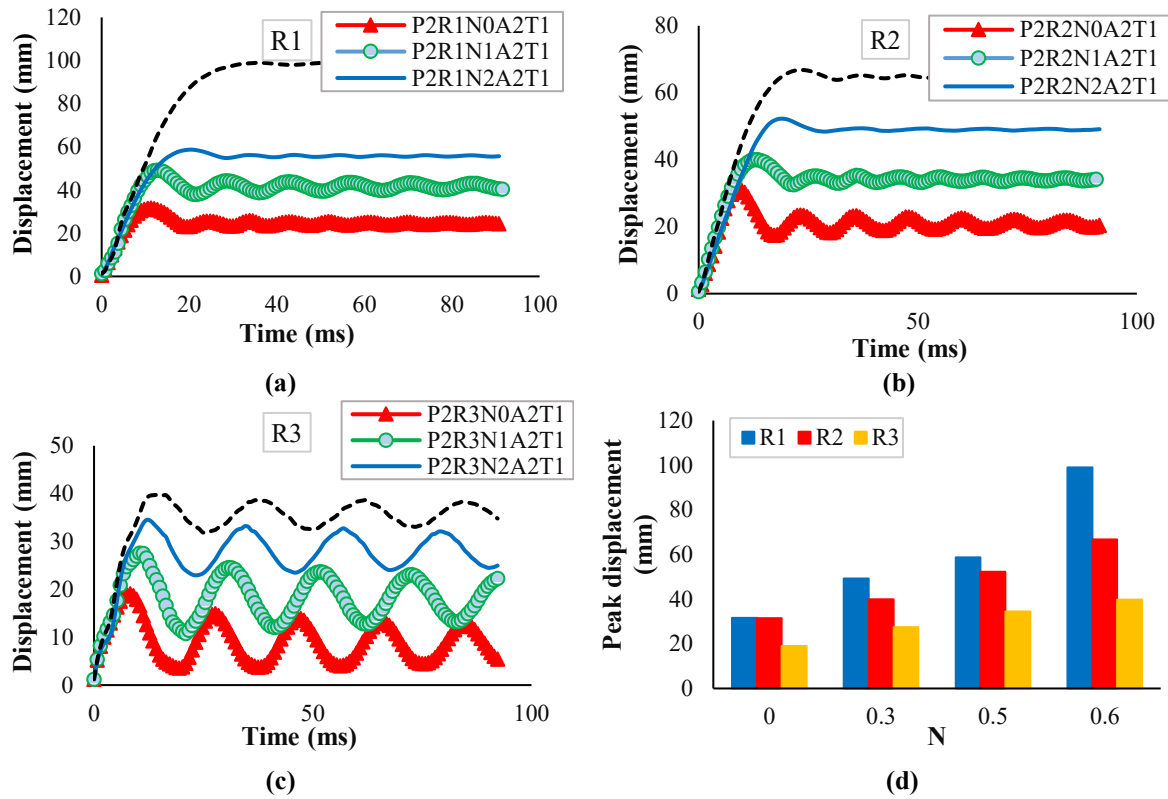


Fig. 15. The displacement - time curves of columns with different axial load ratios: a) Aspect ratio R1; b) Aspect ratio R2; c) Aspect ratio R3; and d) Comparison of peak displacements

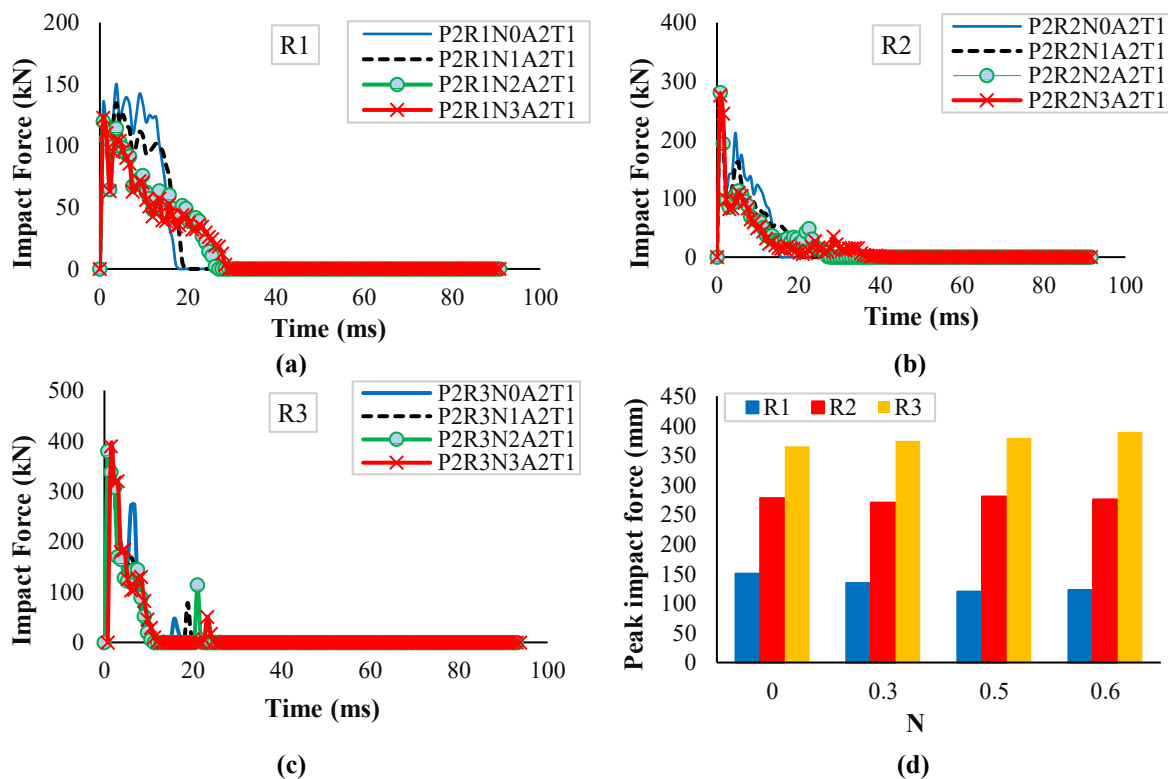


Fig. 16. The impact force-time curves of columns with different axial load ratios: a) Aspect ratio R1; b) Aspect ratio R2; c) Aspect ratio R3; and d) Comparison of peak impact forces

Additionally, the failure modes are illustrated in Figure 17. Based on Figure 15,

the data clearly indicates that the curves exhibit an upward tendency starting from

the time of collision of the impact block t_d . As is observed in Figure 15, the displacements in the column increase with increasing axial load ratio, and in the R1 and R2 aspect ratios, upon the separation of the hit block from the column, the displacements stabilize at a relatively consistent magnitude with a minor oscillation. But in the R3 aspect ratio after the peak point, the displacements are accompanied by more oscillation. The maximum contact time is 34.5 ms, specifically for the P2R1N3A2T1 sample.

The P2R1N3A2T1 specimen exhibits the greatest displacement of 99 mm, while the P2R3N0A2T1 model has the lowest displacement of 19.03 mm. Figure 16 shows the impact force-time curves subjected to an impact load. As depicted in this diagram, when the axial load ratio is increased, the duration of contact between the column and the impact block following the collision is extended, which can be explained by the rise in impact kinetic energy when the axial load ratio is more significant, in which case the column indicates more plastic energy dissipation capacity throughout the impact procedure.

The aspect ratio significantly influences the magnitude of the impact force and by increasing the aspect ratio, can be seen a 69% increase in impact force. The maximal impact force of 518/389 kN is associated with the P2R3N3A2T1 specimen. The bar chart in Figure 16d demonstrates that there is minimal impact on the maximum impact force when the axial load ratio is rose. The

failure modes of the specimens with the R1 aspect ratio for different axial load ratios are illustrated in Figure 17. The figure clearly demonstrates that increasing the axial load ratio increases the specimens' deformation.

4.5. The Effect of Steel Tube Wall Thickness

The primary purpose of this section is to search the influence of the steel tube wall thicknesses (T) on the performance of elliptical hollow and partially concrete-filled cold-formed steel columns under the influence of lateral impact loading. Four thicknesses of 2.25, 2.75, 3.25, and, 4 mm have been selected for the steel tube. The analysis of specimens has been performed by considering the impact angle A2, the filling ratio P2, and the aspect ratios R1, R2 and R3.

The results of the analyses are presented in the procedure of displacement-time curves in Figure 18, impact force-time curves in Figure 19, and failure modes in Figure 20. Based on Figure 18, it is clear that by raising the steel tube's wall thickness, the columns' displacement decreases under the impact load. In the current work, the maximum displacement is related to the P2R1N2A2T0 column with a value of 844.289 mm, and the minimum amount is related to the P2R3N2A2T3 column with a value of 16.065 mm. It is clear from the diagrams in Figure 18d that by increasing the aspect ratio, the columns highest displacement decreases for diverse steel tube wall thicknesses.

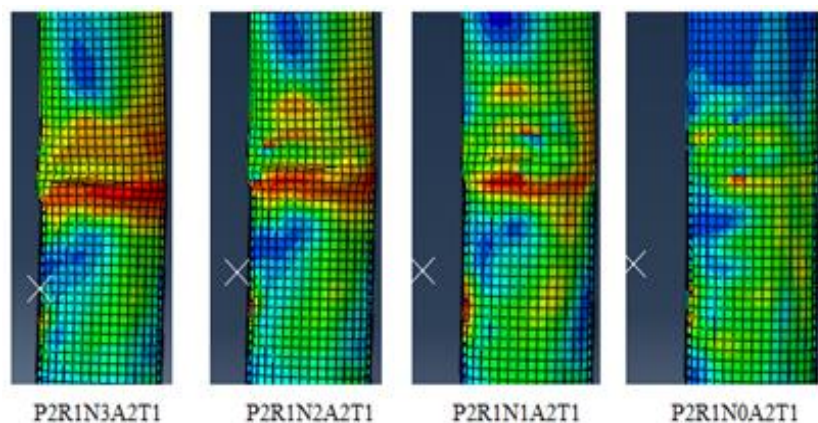


Fig. 17. The failure modes of the columns with R1 aspect ratio for different axial load ratios

At low wall thicknesses of steel tubes, the duration of contact time between the impact block and the column extends after the collision, so the maximum contact time of the P2R1N2A2T0 specimen is 27.751

ms. From the diagrams in Figure 19, it is evident that as the steel tube wall thickness surges, the amount of impact force increases, also the time of complete unloading of the impact load decreases.

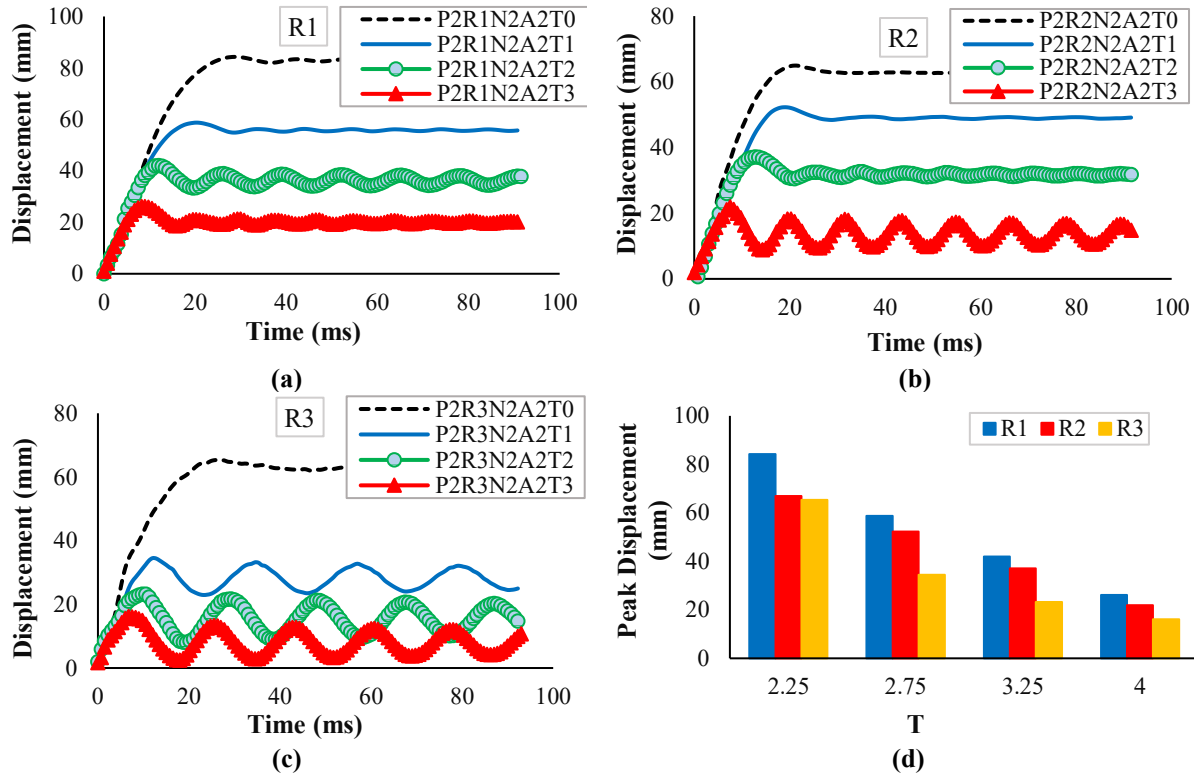


Fig. 18. The displacement - time curves of columns with different wall thicknesses of steel tube: a) Aspect ratio R1; b) Aspect ratio R2; c) Aspect ratio R3; and d) Comparison of peak displacements

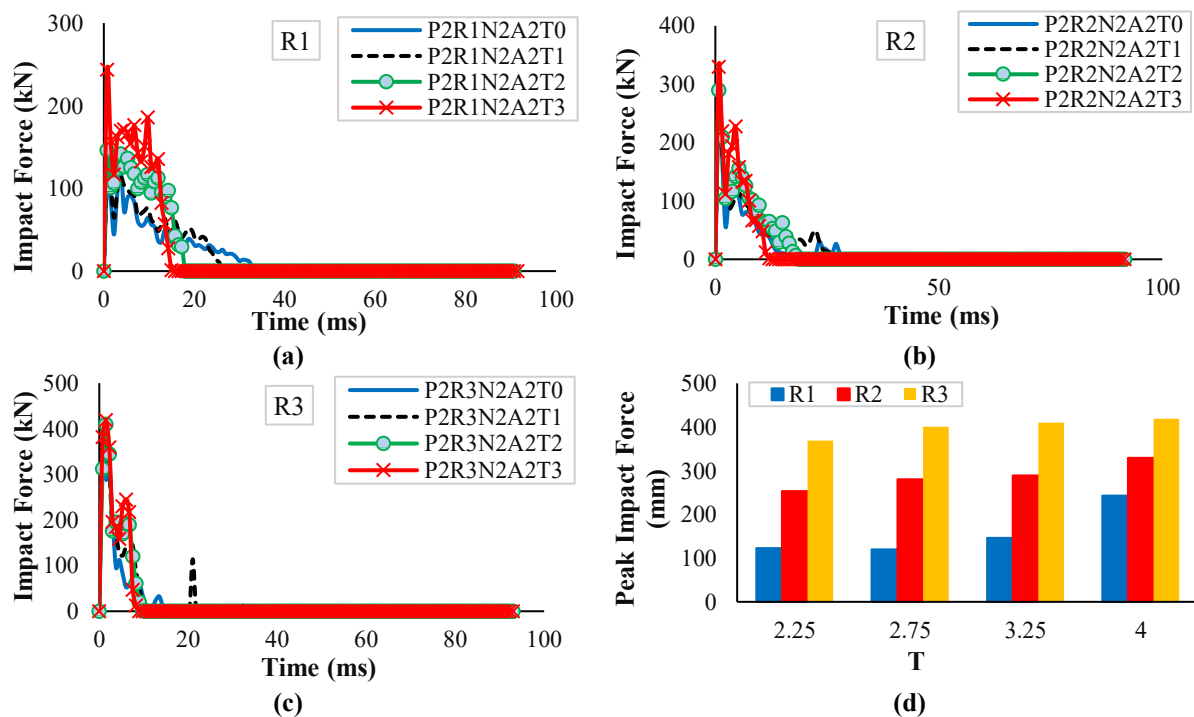


Fig. 19. The impact force-time curves of columns with different wall thicknesses of steel tube: a) Aspect ratio R1; b) Aspect ratio R2; c) Aspect ratio R3; and d) Comparison of peak impact forces

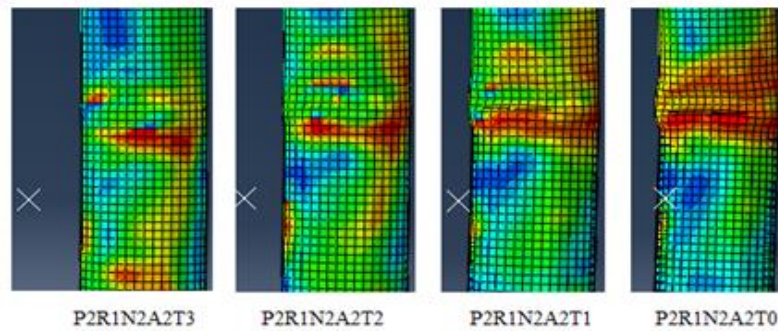


Fig. 20. The failure modes of the columns with the R1 aspect ratio for different thicknesses of steel sections

According to Figure 19d, it can be seen that for different wall thicknesses of steel tubes, the impact force surges with rising the aspect ratio. The maximum impact force of 403.27 kN is associated with the P2R3N2A2T3 specimen. Based on the columns failure modes with the R1 aspect ratio for steel tubes with diverse wall thicknesses in Figure 20, it is evident that more deformation has happened in the columns with low wall thickness.

4.6. The Influence of the Aspect Ratio

The main goal of this section is to investigate the influence of diverse aspect ratios on the performance of elliptical PCFCFST columns. In the current study,

the three different aspect ratios (R) 1.66, 2, and 2.5 are considered. In the previous sections, for each variable parameter, all three aspect ratios are considered. The numerical outcomes of total the considered parameters in this study are assumed in Table 5. On the basis of the outcomes of Table 5, it is clear that in PCFCFST specimens, for changing different parameters, increasing the aspect ratio is associated with decreasing the maximum displacement (Δ_{max}). So the maximum and minimum Δ_{max} are, in turn, related to the aspect ratios R1 and R3, respectively. It can also be seen from the above table that increasing the aspect ratio is associated with decreasing t_d and increasing impact force.

Table 5. The ultimate capacity of the columns with different aspect ratios and filling ratios

Constants		Peak displacement (mm)			t_d (ms)			Impact force (KN)		
		R1	R2	R3	R1	R2	R3	R1	R2	R3
A2, P2, N2	T0	84.2888	66.9254	65.3192	25.7513	19.5011	24.0019	115.6227	253.1291	369.1759
	T1	58.74308	52.2372	34.5086	19.5013	17.2503	9.7501	119.902	280.0948	379.5418
	T2	37.0851	42.0099	23.1753	11.250	10.5013	7.5019	146.0654	289.3365	410.2768
	T3	26.1073	21.8783	16.0648	8.2508	6.0018	3.7517	243.3309	329.6792	419.2018
A2, N2, T1	P0	96.16862	81.02753	86.80809	36.1768	26.2503	24.7523	54.1212	69.0789	75.2334
	P1	91.12152	78.71799	84.81627	33.001	24.7514	24.7507	58.0085	74.7438	72.2073
	P2	58.74308	52.2372	34.50862	19.5013	17.2503	17.2519	119.902	280.6948	379.5418
	P3	35.53408	23.46794	15.67315	12.0003	10.5005	9.7507	177.233	313.7162	408.43
A2, P2, T1	N0	31.57454	31.40822	19.02924	10.5012	7.5016	6.0013	150.2893	280.6948	405.5418
	N1	40.00309	49.21735	27.52239	12.0009	11.2517	8.2502	134.608	277.9797	389.5178
	N2	58.74308	52.2372	34.50862	19.5013	17.2503	9.7501	119.902	275.773	379.5418
	N3	66.79286	98.99415	39.86795	22.5008	34.5007	12.7504	112.5448	270.3577	374.405
P2, N2, T1	A0	53.32463	25.57191	14.49871	18.7502	10.5011	6.0028	110.9875	221.3038	302.3992
	A1	58.74308	52.2372	34.50862	19.5013	17.2503	9.7501	119.902	280.6948	379.5418
	A2	77.79389	75.58222	34.71507	21.7503	23.2501	9.7516	159.902	300.0512	416.8431
	A3	87.89511	86.80803	43.7639	27.7517	26.2503	12.002	205.2967	325.0398	499.8987
	A4	89.85444	88.65604	48.08018	36.7520	29.2504	16.5004	290.6437	348.6568	701.6393

4.7. Discussion

Figure 21 provides the abbreviated numerical results of all the specimens analyzed in. The outcomes of numerical

investigations could be succinctly categorized into five sections based on the parameters under examination.

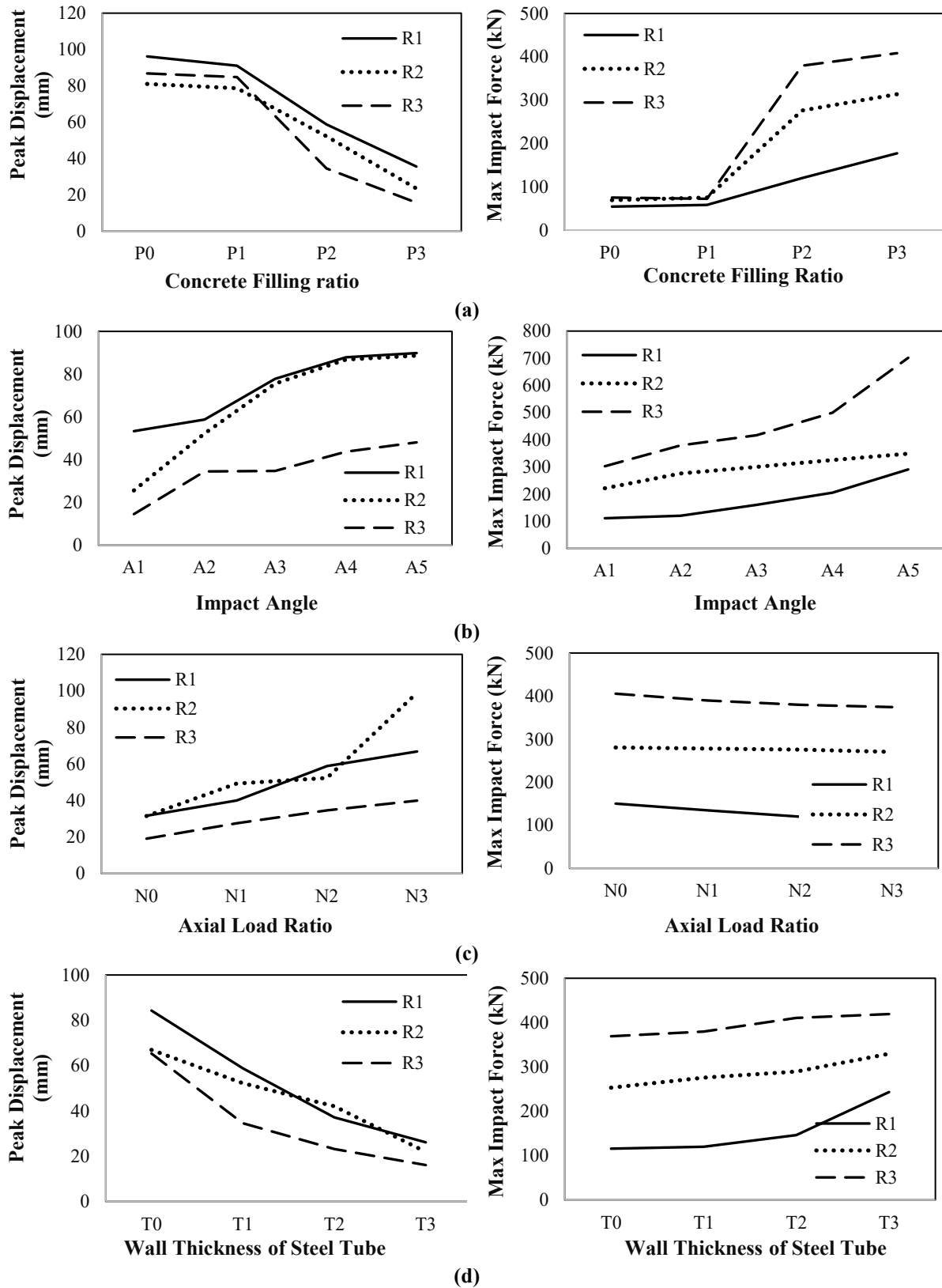


Fig. 21. Numerical results of all the studied specimens

Filling ratio effect: Hollow columns have the highest Δ_{\max} for the different aspect ratios and columns with the highest filling ratio (0.6) have the lowest Δ_{\max} .

Given that the impact height is 0.4 of the column height, the column's performance with a filling ratio of 0.2 is similar to the behavior of an empty column, and the greatest impact force and displacement are approximately the same. By increasing the filling ratio by 0.4, the maximum displacement reduces, and the impact force surges significantly. Swelling the maximum displacement and decreasing the impact force continue with surging the filling ratio to 0.6 with a smooth slope. The outcomes indicate that the lower the filling ratio, the duration of contact between the column and the impact block is longer and the lower the impact load. By surging the filling ratio, the maximum impact force also increases. The maximum displacement in the lower aspect ratio is more significant and gradually reduces with the increasing aspect ratio.

Also, the highest impact force at a lower aspect ratio has the lowest value, which increases with a surging aspect ratio. The difference in the maximum impact force responses for different aspect ratios increases with increasing filling ratio. At larger filling ratios, the influence of the aspect ratio on increasing the maximum impact force is more noticeable.

Impact angle effect: A surge in the greatest amount of displacement and greatest impact force is noticed when the impact angle is altered from zero (along with the big diameter of the ellipse) to 90 degrees (along with the small diameter of

the ellipse). It is also observed that by altering the impact angle from A1 (0) to A5 (90), the increase in displacement in the R3 aspect ratio is much less than the R1 and R2 aspect ratios. The maximum amount of displacements occurs at the impact angle A5 (90) along the small diameter of the elliptical section. It is evident that for all impact angles, the impact force rises with a surging aspect ratio, and for a fixed aspect ratio, the impact force also rises with a rising impact angle from A1 (0) to A5 (90).

Load ratio effect: As the axial force rises, the maximum displacement increases and the impact force decreases linearly with a smooth slope. By surging the axial force from zero to 60% of the ultimate load capacity, at the aspect ratio R3, the maximum impact force decreases by about 8%. This reduction is 4% for the R2 aspect ratio and 25% for the R1 aspect ratio.

Steel tube wall thickness effect: As the wall thickness rises from T0 to T3, the maximum impact force increases and the maximum displacement decreases by approximately 70%. For different wall thicknesses of steel tubes, the impact force surges with rising the aspect ratio.

Aspect ratio effect: In a column with a lower aspect ratio, the maximum displacement is more significant, and the highest impact force is lower. In general, as the cross-sectional aspect ratio rises, the maximum impact force increases, and the greatest displacement decreases. Figure 22 depicts the maximum displacement against the time to reach the maximum displacement.

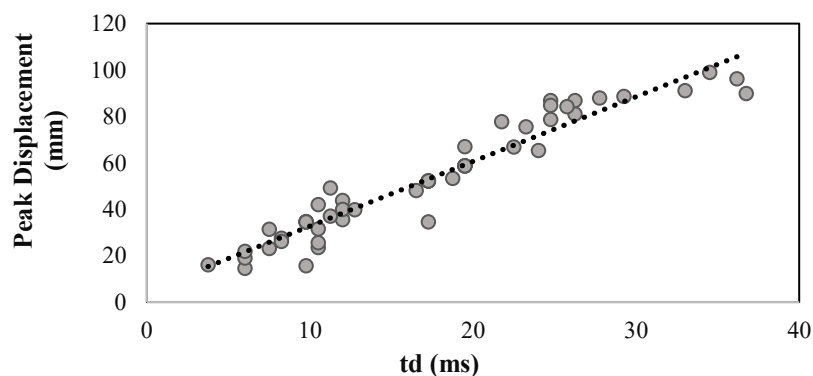


Fig. 22. Scatter of the studied specimen is analysis results

Based on the diagram, it can be determined that there is a nearly linear correlation between the greatest displacement and the time it takes to attain that maximum displacement which follows Eq. (2).

$$\Delta_{max} = 2.8 t_d + 4.85 \quad (2)$$

5. Conclusions

This research investigated the lateral impact behavior of elliptical PCFCFST columns with axial compression load. The influences of aspect ratio, axial load ratio, impact angle, concrete filling ratio, and wall thickness of steel tubes were examined. The primary findings can be succinctly described as follows:

- Hollow columns have the highest Δ_{max} for the different aspect ratios, and columns with the highest filling ratio (0.6) have the lowest Δ_{max} . If an impact is put on the column's hollow part, the behavior of the filled column is the same as that of the empty column. As the filling ratio increases, the greatest displacement decreases, and the highest impact force increases. At larger filling ratios, the effect of the aspect ratio on increasing the highest impact force is more noticeable.
- By changing the impact angle from zero (along with the large diameter of the ellipse) to 90 degrees (along with the small diameter of the ellipse), a surge in the highest displacement and maximum impact force is observed. The maximum amount of displacements occurs at the impact angle A5 (90°) along the small diameter of the elliptical section. For all impact angles, the impact force rises with a surging aspect ratio.
- As the axial force rises, the highest displacement surges and the impact force diminishes linearly with a smooth slope.
- As the wall thickness surges, the highest impact force increases, and the highest displacement decreases. For different wall thicknesses of steel tubes, the impact force increases with the aspect ratio.

- In a column with a lower aspect ratio, the highest displacement is greater, and the highest impact force is lower. In general, as the cross-sectional aspect ratio rises, the maximum impact force increases, and the highest displacement decreases.
- There is a close correlation between the time and maximum displacement it takes to attain that maximum displacement, which can be approximated as a linear relationship.

6. References

- Aghdamy, S., Thambiratnam, D.P., Dhanasekar, M. and Saiedi, S. (2015). "Computer analysis of impact behavior of concrete-filled steel tube columns", *Advances in Engineering Software*, 89, 52-63, <https://doi.org/10.1016/j.advengsoft.2015.06.015>.
- Alam, M.I., Fawzia, S. and Zhao, X.L. (2016). "Numerical investigation of CFRP strengthened full-scale cfst columns subjected to vehicular impact", *Engineering Structures*, 126, 292-310, <https://doi.org/10.1016/j.engstruct.2016.07.058>.
- Baltay, P. and Gjelsvik, A. (1990). "Coefficient of friction for steel on concrete at high normal stress", *Journal of Materials in Civil Engineering*, 2(1), 46-49, [https://doi.org/10.1061/\(ASCE\)0899-1561\(1990\)2:1\(46\)](https://doi.org/10.1061/(ASCE)0899-1561(1990)2:1(46)).
- Craveiro, H.D., Rahnavard, R., Henriques, J. and Simões, R.A. (2022). "Structural fire performance of concrete-filled built-up cold-formed steel columns", *Materials*, 15(6), 2159, <https://doi.org/10.3390/ma15062159>.
- Du, G., Andjelic, A., Li, Z., Lei, Z. and Bie, X. (2018). "Residual axial bearing capacity of concrete-filled circular steel tubular columns after transverse impact", *Applied Sciences*, 8(5), 793, <https://doi.org/10.3390/app8050793>.
- Han, L.H., Xu, C.Y. and Tao, Z. (2019). "Performance of concrete-filled stainless steel tubular columns and joints: Summary of recent research", *Journal of Constructional Steel Research*, 152, 117-131, <https://doi.org/10.1016/j.jcsr.2018.02.038>.
- Liu, F., Wang, Y. and Chan, T.M. (2017). "Behavior of concrete-filled cold-formed elliptical hollow sections with varying aspect ratios", *Thin-walled Structures*, 110, 47-61, <https://doi.org/10.1016/j.tws.2016.10.013>.
- Mohammadi Rana, N., Ghandi, E. and Niari, S.E. (2021). "Lateral impact response of elliptical hollow and partially concrete-filled cold-formed steel columns under static axial compression

- load", *International Journal of Structural Stability and Dynamics*, 2250048, <https://doi.org/10.1142/S0219455422500481>.
- Moradi, M., Tavakoli, H.R. and Abdollahzadeh, G.R. (2021). "Comparison of steel and reinforced concrete frames' durability under fire and post-earthquake fire scenario", *Civil Engineering Infrastructures Journal*, 54(1), 145-168, [10.22059/CEIJ.2020.292639.1628](https://doi.org/10.22059/CEIJ.2020.292639.1628).
- Rahnavard, R., Craveiro, H.D., Simões, R.A., Laim, L. and Santiago, A. (2022a). "Fire resistance of concrete-filled cold-formed steel built-up short columns", *Journal of Building Engineering*, 48, 103854, <https://doi.org/10.1016/j.jobe.2021.103854>.
- Rahnavard, R., Craveiro, H.D., Lopes, M., Simões, R.A., Laim, L. and Rebelo, C. (2022b). "Concrete-filled cold-formed steel built-up columns under compression: Test and design", *Thin-Walled Structures*, 179, 109603, <https://doi.org/10.1016/j.tws.2022.109603>.
- Rahnavard, R., Craveiro, H.D. and Simões, R.A. (2023). "Analytical prediction of the axial capacity of concrete-filled cold-formed steel built-up columns", *In Proceedings of the Annual Stability Conference*, Charlotte, North Carolina, 188, 110792, <https://doi.org/10.1016/j.tws.2023.110792>.
- Rondal, J. (2000). "Cold-formed steel members and structures: general report", *Journal of constructional steel research*, 55(1-3), 155-158, [https://doi.org/10.1016/S0143-974X\(99\)00083-8](https://doi.org/10.1016/S0143-974X(99)00083-8).
- Shakir, A.S., Guan, Z.W. and Jones, S.W. (2016). "Lateral impact response of the concrete-filled steel tube columns with and without cfrp strengthening", *Engineering Structures*, 116, 148-162, <https://doi.org/10.1016/j.engstruct.2016.02.047>.
- Wan, J., Chen, Y., Wang, K. and Han, S. (2017). "Residual strength of chs short steel columns after lateral impact", *Thin-Walled Structures*, 118, 23-36, <https://doi.org/10.1016/j.tws.2017.04.027>.
- Wang, Y., Qian, X., Liew, J.R. and Zhang, M.H. (2015). "Impact of cement composite filled steel tubes: an experimental, numerical and theoretical treatise", *Thin-Walled Structures*, 87, 76-88, <https://doi.org/10.1016/j.tws.2014.11.007>.
- Wang, J., Shen, Q., Jiang, H. and Pan, X. (2018). "Analysis and design of elliptical concrete-filled thin-walled steel stub columns under axial compression", *International Journal of Steel Structures*, 18(2), 365-380, <https://doi.org/10.1007/s13296-018-0002-5>.
- Xu, W., Zhu, A.Z. and Gao, K. (2018). "Parameter analysis on the anti-impact behavior of pcfst columns under lateral impact load", *In MATEC Web of Conferences*, 206, 01020, <https://doi.org/10.1051/mateconf/201820601020>.
- Yang, Y.F., Zhang, Z.C. and Fu, F. (2015). "Experimental and numerical study on square rcfst members under lateral impact loading", *Journal of Constructional Steel Research*, 111, 43-56, <https://doi.org/10.1016/j.jcsr.2015.04.004>.
- Yang, H., Liu, F., Chan, T.M. and Wang, W. (2017). "Behaviors of concrete-filled cold-formed elliptical hollow section beam-columns with varying aspect ratios", *Thin-Walled Structures*, 120, 9-28, <https://doi.org/10.1016/j.tws.2016.10.013>.
- Yousuf, M., Uy, B., Tao, Z., Remennikov, A. and Liew, J.R. (2014). "Impact behavior of pre-compressed hollow and concrete filled mild and stainless steel columns", *Journal of Constructional Steel Research*, 96, 54-68, <https://doi.org/10.1016/j.jcsr.2013.12.009>.
- Yu, W.W. (2000). "Cold-formed steel design", Ph.D. Thesis, University of Missouri-Rolla, <https://www.wiley.com/en-us/cold-formed+steel+design%2c+5th+edition-p-9781119487418>.
- Zhang, X., Chen, Y., Shen, X. and Zhu, Y. (2019). "Behavior of circular cfst columns subjected to different lateral impact energy", *Applied Sciences*, 9(6), 1134, <https://doi.org/10.3390/app9061134>.
- Zhu, A.Z., Xu, W., Gao, K., Ge, H.B. and Zhu, J.H. (2018). "Lateral impact response of rectangular hollow and partially concrete-filled steel tubular columns", *Thin-Walled Structures*, 130, 114-131, <https://doi.org/10.1016/j.tws.2018.05.009>.



This article is an open-access article distributed under the terms and conditions of the Creative Commons Attribution (CC-BY) license.